Analysis of plant root-induced preferential flow and pore-water pressure variation by a dual-permeability model

Shao, Wei; Ni, Junjun; Leung, Anthony Kwan; Su, Ye; Ng, Charles Wang Wai

DOI
10.1139/cgj-2016-0629

Publication date
2017

Document Version
Accepted author manuscript

Published in
Canadian Geotechnical Journal

Citation (APA)
Shao, W., Ni, J., Leung, A. K., Su, Y., & Ng, C. W. W. (2017). Analysis of plant root-induced preferential flow and pore-water pressure variation by a dual-permeability model. *Canadian Geotechnical Journal*, *54*(11), 1537-1552. https://doi.org/10.1139/cgj-2016-0629

Canadian Science Publishing
NRC Research Press journals | Publishing Services

Canadian Geotechnical Journal
Revue canadienne de géotechnique

Analysis of plant root-induced preferential flow and pore water pressure variation by a dual-permeability model

Journal:	*Canadian Geotechnical Journal*
Manuscript ID	cgj-2016-0629
Manuscript Type:	Article
Date Submitted by the Author:	19-Nov-2016
Complete List of Authors:	Shao, Wei; Technische Universiteit Delft Ni, Junjun; The Hong Kong University of Science and Technology, Department of Civil and Environmental Engineering Leung, Anthony; University of Dundee, Division of Civil Engineering Su, Ye; charles university in prague Ng, Charles Wang Wai; Hong Kong University of Science and Technology
Keyword:	planting density, suction, preferential flow, dual-permeability model, slope stability

Analysis of plant root-induced preferential flow and pore water pressure variation by a dual-permeability model

Wei SHAO[1, 2], Junjun NI [1*], Anthony Kwan LEUNG[3], Ye SU[4], Charles Wang Wai NG[1]

1 Department of Civil and Environmental Engineering, The Hong Kong University of Science and Technology

2 Water Resources Section, Faculty of Civil Engineering and Geosciences, Delft University of Technology, 2628CN, Delft, Netherlands

3 School of Science and Engineering, University of Dundee, UK

4 Department of Physical Geography and Geoecology, Faculty of Science, Charles University in Prague, 12843, Prague, Czech Republic

[*] Corresponding author (Email: jniaa@ust.hk)

Abstract

Vegetation can affect slope hydrology and stability via plant transpiration and its induced matric suction. Previous work suggested that the presence of plant roots would induce preferential flow, and its effects may be more significant when the planting density is high. However, there is a lack of numerical study on how planting density affects soil pore water pressure and shear strength during heavy rainfall. This study aims to investigate the impact of plant root-induced preferential flow on hydro-mechanical processes of vegetated soils under different planting densities. Two modelling approaches, namely single- and dual-permeability models, were integrated with an infinite slope stability approach to simulate pore water pressure dynamics and slope stability. Laboratory tests on soils with two different planting densities for a plant species, *Schefflera heptaphylla*, were conducted for numerical simulations. Decayed roots were found to be more evident in the high planting density soil. The single-permeability model overestimated the pore water pressure in shallow soil and underestimated the infiltration depth. The dual-permeability model, which is able to model the effects of preferential flow, can better capture the observations of rapid increase of pore water pressure and deeper pressure response in the vegetated soil. However, caution should be taken on the choice of pore water pressure when using the dual-permeability model to assess the factor of safety. The dual-permeability model using the pore water pressure in the preferential flow domain and that in the matrix domain would result in lower and higher factor of safety, respectively.

Keywords: planting density; suction; preferential flow; dual-permeability model; slope stability

1. Introduction

Vegetation has been recognised as an environmentally friendly restoration technique for slope stabilization. On one hand, due to the mechanical reinforcement of plant root system, the tensile strength provided by roots at the potential slip surface of a slope increases soil shear strength, which may be used to stabilize the landslide-prone areas (Cohen et al. 2009). On the other hand, plant transpiration and root water uptake can induce soil matric suction (equal to negative pore water pressure in unsaturated soils), resulting in an increase in soil shear strength (Ng and Menzies 2007) and a decrease in soil hydraulic conductivity (Leung et al. 2016; Ng and Leung 2012).

Slope restoration is affected by growing and decaying of roots, which would consequently cause changes in both soil hydraulic and mechanical properties (Lehmann and Or 2012). Due to plant life cycle and competition among plants, growing and decaying of roots may lead to changes in tensile strength for the root reinforcement (Cohen et al. 2009). Besides, root occupation and biodegradation has been shown to significantly affect the soil hydraulic properties such as soil water retention curve and saturated hydraulic conductivity (Li and Ghodrati 1994; Scholl et al. 2014; Leung et al. 2015a, b; Vergani and Graf 2015; Ng et al. 2016a). The pattern of infiltration and associated soil moisture and pore water pressure dynamics would therefore be affected by root physiological processes (Snyder et al. 2003).

Planting density is an important factor influencing the physiological processes of root in terms of growing and decaying, and therefore altering the effectiveness of slope restoration. Low planting density leads to low root biomass production, resulting in a reduction of root reinforcement and root water uptake (Ng et al. 2016b). In contrast, high planting density induces higher transpiration during an intermittent period between rainfall events, causing a greater increase in matric suction in root zone. In addition, high planting density may lead to the competition for water, nutrients, and light among neighbouring plants, which could consequently hamper root biomass production, resulting in root decaying (Azam – Ali et al. 1984; Darawsheh et al. 2009; Benomar et al. 2012; Ng et al. 2016b).

Recent studies reported by Ng et al. (2016a, b) found that the growth of plant was accompanied with root biomass production, affecting the root occupancy of soil pore space. As a result, for the case of low planting density, vegetated soil may have relatively lower soil hydraulic conductivity and higher water retention ability than bare soil (Scanlan and Hinz

2010; Scholl et al. 2014; Leung et al. 2015b; Ng et al. 2016b). In contrast, for the case of high planting density, the presence of decayed roots would increase the saturated hydraulic conductivity and reduce the water retention ability (Ng et al. 2016b).

Decayed root channels can compose a self-organized macropores network, in which the preferential flow may be triggered under high-intensity rainfall or wet soil moisture condition (Sidle et al.2001; Jarivs 2007; Ghestem et al. 2011; Nimmo 2012). The rainfall may infiltrate through the interconnected root channels, resulting in rapid water movement and pore water pressure response in deep soil (Beven and Germann 2013). Even in an individual macropore, which is not directly connected to surface infiltration or ponded water, the hydraulic connection can be achieved by pressure propagation and water exchange between macropores and matrix (Nimmo 2007; Nieber and Sidle 2010). Preferential flow can affect tracer transport in terms of reducing travel time, increasing infiltration depth, and affecting concentrations in drainage flow (Jarvis 2007; Beven and Germann 2013). Particularly, under heavy rainfall or snow-melting conditions, the occurrence of preferential flow in a potentially unstable slope could cause rapid infiltration and percolation (Uchida 2004; Shao et al. 2015). Consequently, preferential flow induces fast pore water pressure change at the potential slip surface, and this could play an important role in triggering slope failure (Van Asch et al. 1999; Hencher 2010; Sidle and Bogaard 2016).

The commonly-used numerical models for coupling seepage and slope stability analysis are single-permeability models, which employ the Darcy-Richards equation or its various simplification (e.g., the linear diffusion equation, Boussinesq equations) in an assumed single-continuum soil(Iverson 2000; Talebi et al. 2008; Lu et al. 2012). A single-permeability model often neglects the effects of preferential flow, so it could underestimate the amount of infiltration, percolation, and drainage in slopes during heavy rainfall (Beven and Germann 2013). Existing numerical studies indicate that the single-permeability model is unable to correctly simulate rapid water and tracer movement in macropore soils (Jarvis 2007; Köhne et al. 2009). Recent studies also suggested that even though the equivalent parameter sets were used by the single-permeability model, it is still not possible to simulate fast pressure response and the associated effects on slope stability (Shao et al. 2015, 2016).

It is a remaining challenge on how to deterministically quantify the impact of preferential flow on slope hydrology and stability (Uchida 2004; Hencher 2010; Bogaard and Greco 2016). Many preferential flow models have been developed such as a pore-network model, dual- or

multi-continuum conceptualization of soil porous medium (see review by Köhne et al. (2009)). Specifically, the dual-permeability model uses two coupled Darcy-Richard equations (Gerke and Köhne 2004; Köhne et al. 2009) to quantify the dual-effect of the matrix and preferential flow on infiltration, pressure propagation, and their effects on slope stability (Shao et al. 2015, 2016). Application of such dual-permeability model for an ecological system may be necessary to simulate the hydrological and mechanical responses of soils with widespread decayed roots that potentially form a macropore network.

This study aims to quantify the impact of planting density on soil hydrology, including the response in pressure propagation and their effects on soil mechanical responses and slope stability. Numerical modelling and analyses were conducted to simulate and back-analyse the recent experiments reported by Ng et al. (2016b). In the experiments, a tree species, *Schefflera heptaphylla,* with ornamental and ecological value for slope rehabilitation and reforestation was tested. The species were planted in big drums with different planting densities. Root area index was measured to quantify the effects of planting density on root growth and decay. The measured variation of soil pore water pressure during a rainfall event was simulated using both the single- and dual-permeability models. Subsequently, the role of planting density on slope stability was analysed.

2. Laboratory test

2.1 Test plan, test setup and instrumentation

Two different planting densities of 36 (test D36), and 320 (test D320) seedlings/m^2, corresponding to the plant spacing of 0.18 m and 0.06 m were investigated (Ng et al. 2016b). Each planting density was tested with three replicates. There were six drums in total for testing vegetated soils, each of which has a diameter of 0.6 m and a height of 0.5 m. An additional drum was compacted with bare soil for measuring soil water retention curve and saturated hydraulic conductivity. Multiple-holes were made in the bottom of each drum for creating a free drainage boundary. The targeted plant species, *Schefflera heptaphylla,* is small-sized, and semi-deciduous. Plant individuals were transplanted to the test drums with a uniform spacing at the targeted plant densities (Figure 1).

The tested soil was completely decomposed granite (CDG) that can be classified as silty sand according to the Unified Soil Classification System (USCS; ASTM, 2010). The CDG was compacted at a dry density of 1780 kg/m^3 for all the test drums. Two vertical arrays of

miniature-tip tensiometers were installed at the depth of 0.05, 0.10, 0.15, 0.25, and 0.35 m to measure the negative pore water pressure. An array of tensiometers (denoted by R) was located in the middle of the drum that is beneath a tree individual. Another array (denoted by M) was installed next to the array R with a distance of half-spacing. The volumetric water content at depth of 0.05 m and 0.10 m was measured by two soil moisture probes (SM300, Delta-T Device Ltd).

All test drums were placed in a plant room with well-controlled environmental condition. The air temperature and relative humidity were maintained at 25±1°C and 60±5%, respectively. The radiation energy was provided by the cool white fluorescent lamp with irradiance of 5.0 $MJ/m^2/day$, and the wave band was within the range of 400-700 nm to promote the plant growth (Ng et al. 2014). Irrigations were applied frequently to maintain the average soil moisture that was close to the field capacity, which is commonly considered to be sufficient for root growth (Wang et al. 2007).

2.2 Test procedures

A two-stage test was conducted after a 4-month growing period. The first stage was to saturate the drums with a constant ponding head until the soil in each drum was fully-saturated. Afterward, the ponding water was removed and all the drums were exposed to a 4-day drying period under the same atmospheric condition. The second stage was commenced immediately after the drying test. Artificial rainfall was applied with a controlled intensity of 73 mm/h and duration of 2 h, corresponding to a 10-year return period in Hong Kong (Lam and Leung 1995). All the drums were inclined at a small angle of 2° to ensure that any water ponded on the soil surface during rainfall could turn into infiltration-excess overland flow. The distributions of pore water pressure in all drums were recorded at a 10-min interval during the second stage infiltration tests.

After the infiltration test was completed, all plants were carefully removed from each drum. The roots were cleaned to investigate the geometry of root system. The detailed procedures can refer to Ng et al. (2016b). The rooting depth is defined as the deepest soil depth, beyond which no root can be found. Root area index (RAI) is defined as the ratio of the total root surface area to the cross-section area of soil for a given depth. The ImageJ software was used to reconstruct the root system with high-resolution images (i.e., 12 pixels per unit mm of

length). The root surface area of each cross-section was calculated by converting the pixel number into surface area of roots in mm^2.

The measured RAI distribution with soil depth and typical root systems obtained at different planting densities are shown in Figure 2. All the root systems were in parabolic shape along depth. The root system from the test D36 was more dispersed. The average rooting depth in test D36 was 0.16 m, which was 30% longer than that in test D320 (i.e., 0.125 m). However, the largest RAI values of test D320 (i.e., 0.7) was 40% larger than test D36 (i.e., 0.5). Interestingly, in all the repeated tests, the decayed roots were commonly found in soil of test D320, while the roots in test D36 were mainly fresh and less decayed roots were observed.

3. Mathematical models

The models described herein aim to capture and simulate the transient infiltration processes and pore water pressure dynamics in a one-dimensional (1D) profile of vegetated soil. For modelling simplicity, the roots in each tested drum are considered to be homogeneously distributed within the root zone. As it has been shown by Ng et al. (2016b) that any plant transpiration during the short 2 h rainfall event in the drum tests was minimal, it is reasonable to ignore the plant transpiration as well as soil evaporation in the calculation (Sidle et al.1985; Snyder et al.2003). In this study, the effects of roots on infiltration are represented by the parameterisation of the soil hydraulic parameters, including soil water retention curve and saturated hydraulic conductivity (Leung et al. 2015a, b; Ng et al. 2014, 2016a, b).

3.1 Single-permeability model

The single-permeability model uses one Darcy-Richards equation to simulate the transient response of pore water pressure to rain-pulses:

$$C\frac{\partial h}{\partial t}=\frac{\partial}{\partial z}\left[K\left(\frac{\partial h}{\partial z}+1\right)\right]-\Gamma \qquad (1)$$

where t (T) is time, θ (L^3L^{-3}) is the water content, C ($d\theta/dh$) (L^{-1}) is the differential water capacity, h (L) is the pressure head, K (LT^{-1}) is the unsaturated hydraulic conductivity, and Γ (T^{-1}) is the source or sink term that may be used to calculate root water uptake (Feddes 1976; Leung et al. 2015a, b) and soil evaporation (if a longer term of soil moisture dry-down and

pressure recession was to be modelled). In this study, the term Γ is set to be zero, considering that the plant transpiration during the short period of rainfall (2 h) is negligible (Snyder et al. 2003).

The Mualem-van Genuchten model is used to describe the hydraulic properties of vegetated soils (Van Genuchten 1980):

$$\Theta = \frac{\theta - \theta_r}{\theta_s - \theta_r} = \begin{cases} \left[1 + |\alpha h|^n\right]^{-m}, & h < 0 \\ 1, & h \geq 0 \end{cases} \quad (2)$$

$$C(\Theta) = \begin{cases} mn\alpha\left(\theta_s - \theta_r\right)\Theta^{1/m}\left(1 - \Theta^{1/m}\right)^m, & h < 0 \\ S_s, & h \geq 0 \end{cases} \quad (3)$$

$$K(\Theta) = K_s\Theta^{0.5}\left[1 - \left(1 - \Theta^{1/m}\right)^m\right]^2 \quad (4)$$

where Θ (-) is the effective saturation, θ (L^3L^{-3}) is the volumetric water content, subscript r and s denote residual and saturated state, S_s (L^{-1}) is the specific storage in saturated soil, and α (L^{-1}), n (-), and m (-) are the fitting parameters.

The boundary condition of the single-permeability model can be specified as the flux of rainfall intensity or pressure head for ponding condition. The switch between the two boundary conditions are achieved by theories and formula referring to van Dam and Feddes (2000).

3.2 Dual-permeability model

The dual-permeability model uses two Darcy-Richards equations to simultaneously simulate the non-equilibrium phenomenon that is caused by the different pore water flow velocities in preferential flow paths and in soil matrix (Gerke and van Genuchten 1993):

$$C_f\frac{\partial h_f}{\partial t} = \frac{\partial}{\partial z}\left[K_f\left(\frac{\partial h_f}{\partial z} + 1\right)\right] - \frac{\Gamma_w}{w_f} \quad (5)$$

$$C_m\frac{\partial h_m}{\partial t} = \frac{\partial}{\partial z}\left[K_m\left(\frac{\partial h_m}{\partial z} + 1\right)\right] + \frac{\Gamma_w}{w_m} \quad (6)$$

where the subscript f indicates the preferential flow domain, the subscript m indicates the matrix domain, w (-) is the volume fraction of the preferential flow domain or the matrix domain, and Γ_w (T^{-1}) is the water exchange term (Gerke and van Genuchten 1993):

$$\Gamma_w = \alpha_w \frac{K_m(h_f) + K_m(h_m)}{2}(h_f - h_m) \tag{7}$$

where α_w (L^{-2}) is the water exchange coefficient.

The soil hydraulic characteristics of both matrix and preferential flow domain are described by the Mualem-van Genuchten model (Van Genuchten 1980). The total effect adopts the Durner's formula (Durner 1994). The volumetric ratio of the preferential flow and matrix flow sums up to one:

$$w_f + w_m = 1 \tag{8}$$

The total volumetric water content of the soil is the weighted average of volumetric water contents in two domains:

$$\theta = w_f \theta_f + w_m \theta_m \tag{9}$$

The same holds for the total saturated hydraulic conductivity of the soil:

$$K_S = w_f K_{Sf} + w_m K_{Sm} \tag{10}$$

The boundary conditions of the Darcy-Richards equation could be specified as pressure head, flux, or mixed. The specified infiltration flux i (LT^{-1}) on the dual-permeability soil surface can be divided into two constituting domains (Dusek et al. 2008):

$$i = w_f i_f + w_m i_m \tag{11}$$

where i_f and i_m are specified boundary fluxes on the surface of matrix domain and preferential flow domain.

The preferential flow may not to be triggered at the beginning of a rainfall event; consequently, and the infiltration only starts in the matrix domain (Shao et al. 2016), expressing as:

$$R = i = w_m i_m \tag{12}$$

If the specified flow at the matrix surface exceeds its infiltration capacity, the boundary condition of the matrix domain would change to a specified pressure head. Hereafter, the

infiltration-excess water at that time-step would be reallocated to the surface boundary of the preferential flow domain:

$$i_f = \frac{R - w_m i_m}{w_f} \tag{13}$$

If the specified flux for the preferential flow domain is larger than its infiltration capacity, the boundary conditions of both domains would switch to a specified pressure head that corresponds to the depth of ponding water on soil surface.

3.3 Infinite slope stability calculation

In order to investigate the effects of planting density on the slope stability, an infinite slope stability calculation is carried out, considering that the slope is vegetated with *Schefflera heptaphylla* under the two planting densities in the drum tests. The hydrological processes in the infinite slope are assumed to be the same as what the soils experienced in the drum tests. The factor of safety F_s is expressed as the ratio of resisting force to gravitationally driving force with three terms (Lu and Godt 2008):

$$F_s(z_H) = \underbrace{\frac{\tan\phi'}{\tan\alpha}}_{\text{friction angle term}} + \underbrace{\frac{c'}{G\sin\alpha\cos\alpha}}_{\text{cohesion term}} - \underbrace{\frac{\sigma^s}{G}\frac{\tan\phi'}{\sin\alpha\cos\alpha}}_{\text{suction stress term}} \tag{14}$$

where z_H (L) is the depth below the slope surface considered for slope stability calculation, c' ($ML^{-1}T^{-2}$) is the effective soil cohesion, ϕ' (deg) is the friction angle, α (deg) is the slope angle, and G ($ML^{-1}T^{-2}$) is weight of soil:

$$G = \int_{z_H}^{H} \left[\gamma_s + \gamma_w \theta\right] dz \tag{15}$$

where γ_s and γ_w ($ML^{-2}T^{-2}$) are the specific weight of dry soil and water.

The suction stress σ^s ($ML^{-1}T^{-2}$) is given as:

$$\sigma^s = \chi p_w = \chi \gamma_w h \tag{16}$$

where p_w($ML^{-1}T^{-2}$) is the pore water pressure, and χ (-) is the matrix suction coefficient, which may be approximated by the effective saturation (Lu et al. 2010).

The hydrological results were sequentially coupled with the soil mechanical calculations in the following ways. The unit self-weight of soil was related to the soil moisture distribution (Eq. (15)). The suction stress and shear strength were influenced by pore water pressure and effective saturation. In the dual-permeability model, the pore water pressure head obtained from either preferential flow domain, or matrix domain, or their weighting may be used as an "effective pressure" (p_{eff}) for the slope stability analysis. Shao et al. (2015, 2016) selected the pressure of the preferential flow model for stability calculation. This method considered that the infiltration and pressure build-up in preferential flow paths reached a given depth of slope failure plane, hence giving a relatively conservative estimation of slope stability. The simulation conducted in the present study investigated the sensitivity of the choice of p_{eff} to the F_s calculation, using (i) pressure from the preferential flow domain (p_f); (ii) pressure from the matrix domain (p_m); and (iii) the arithmetic mean of the pressure between the two domains (i.e., 0.5*(p_f + p_m)). It should be noted that as far as the authors are aware, there is no theoretical model available to determine the exact weighting of pressure between the two domains that would affect soil shear strength. The scenario (iii) aims to explore how the combined effects of the two domains would affect the assessment of slope stability.

4. Model implementation and parameterization

4.1 Numerical models and parameterization strategies

The mathematical models were numerically solved by an author-developed script under Python 2.7 programming environment (Shao et al. 2016). The Darcy-Richards equation of single- and dual- permeability models was solved by an implicit finite difference method (van Dam and Feddes 2000; Simunek et al. 2005). The Picard iteration technique was used for each time step. For ensuring numerical accuracy and computational efficiency during the computation, the tolerable errors of water content were specified with 0.0001, and the time step was adapted in a range of 0.02~5 min.

A uniform computational grid of 0.01 m was used to discretize the soil of 0.45 m depth. Both the single- and dual- permeability models were used to simulate the infiltration tests. In both models, the initial pressure head distribution before the infiltration tests was obtained by the

interpolation of the measured pore water pressure head right after the 4-day drying period. Rainfall pulse with the intensity of 73 mm/h was set as the upper boundary condition, while the boundaries may switch to the pressure head boundary with a ponding depth of 0.1 mm under such high-intensity rainfall.

The soil hydraulic parameters were manually calibrated for two layers. The first layer was from the soil surface to the rooting depth (i.e., root zone), in which the soil hydraulic properties were affected by the presence of living and decayed roots. Below the root zone where the soil was less affected by vegetation, the soil hydraulic parameters may be specified to be the same as the bare soil. For numerical simulations, the following calibration strategies were sequentially used to parameterize the models: (1) the soil water retention curves were estimated according to the measurements of soil moisture and pore water pressure; (2) the saturated hydraulic conductivities were estimated according to the measured infiltration rate; and (3) for the dual-permeability model, the water exchange coefficients were estimated according to the measured pore water pressure response. The hydraulic parameters for soils in different experiment cases are listed in Table 1.

4.2 Water retention curve

The soil water retention curves (SWRCs) for single- and dual- permeability model were determined according to water content and pore water pressure as shown in Figure 3. The data points of water content and pressure head can be classified into two categories - drying series and wetting series, depending on whether the data was from the first-stage drying period or the second-stage infiltration period. In the bare soil, the difference between drying and wetting curves is indiscernible. On the contrary, more significant hydraulic hysteresis was found in the vegetated soils (regardless of the planting density). For pore water pressure ranged from 0 to -10 kPa, the changes of water content during the wetting process is generally smaller than that during the drying process, probably because of the presence of macropores.

For the single-permeability model, bare soil and vegetated soils (test D320 and D36) have the same values of θ_r (0.1) and θ_s (0.3). Both parameters, α and n , controlling the shape of SWRC, were fitted by the nonlinear least-squares algorithms using the sqcurvefit function in Matlab. The fitted SWRC for bare soil and vegetated soils from single-permeability model are shown in Figures 3 a, b, d, respectively, with all the fitting parameters shown in Table 1. Both

the n and α for the case of high planting density (D320) are relatively larger, which tend to behave like a coarser soil.

The composite SWRC determined by the dual-permeability function is shown in Figures 3 c, e. The composite SWRC has two groups of parameters to describe the different hydraulic characteristics of the matrix and preferential flow domains. The parameters (θ and w) for the volumetric ratio ($w(\theta_s - \theta_r)$) of the matrix and preferential flow domains were predefined, according to the measured root volume. The θ_s for the preferential flow domain was thus set to be 0.39 considering the occupancy of decayed roots in soil pore space (Ng et al. 2016b), while the θ_s for the matrix domain is calculated according to Eq. 9. The volumetric ratio of the preferential flow domain w_f commonly ranges from 0.025 to 0.2. Note that different choices of w_f may result in equifinal parameter sets of SWRCs. This means that different parameter sets of the dual-permeability model could result in the same composite SWRC of the total domain for the dual-permeability model (Köhne et al. 2002). In this study, predefined values of w_f were set to be 0.1 and 0.2 for the low and high planting density soils, respectively. This means that the volumetric ratio of soil pores, $w_f(\theta_{sf} - \theta_{rf})$ belonging to the preferential flow domains for the low and high planting density soil is about 3% and 6%, respectively. A relatively higher value of w_f was specified for the high planting density soil for taking into account the effects of decayed roots (Figure 2). The validity of the use of a higher volumetric ratio w_f is discussed in the infiltration analysis later (Section 5.1).

For the dual-permeability model, the parameters, α and n, of the two domains are optimized by the sqcurvefit function. These two parameters sets of the SWRC fitted for the matrix domain of the dual-permeability model can be used to describe the measured water retention behavior of the total domain, given the reasonably good agreement shown in Figures 3c, e. The parameter n in the preferential flow domain was calibrated to be 1.5 for both D36 and D320 soils according to the shapes of SWRC. On the other hand, α is related to the air entry pressure, and the specified value for D36 and D320 is 6 and 10 m^{-1}, respectively. For the deeper soil layer beyond the root zone, the soil hydraulic properties may not be affected by root growth and decaying, and the parameters of α and n of both the matrix and preferential flow domains thus followed the same parameters of bare soil.

4.3 Saturated hydraulic conductivity and water exchange coefficient

The values of K_s were calibrated based on the results obtained from the infiltration test. The calibrated K_s of the bare soil is found to be 0.075 m/day when using the single-permeability model. For the vegetated soils, the calibrated K_s for the high planting density soil (D320; 0.175 m/day) is higher than that for the low planting density soil (D36; 0.06 m/day). This is consistent with the experimental observation in Figure 2 that the high planting density soil contained more decayed roots. The decayed roots can affect the soil hydraulic behavior via the changes in the shape of SWRC (Figure 3) and also lead to an increase in K_s (Table 1).

When using the dual-permeability model, the saturated hydraulic conductivity of the preferential flow domain K_{sf} was set to be 4.5 m/day, which is 300 and 60 times larger than K_{sm} for the case of low and high planting density, respectively. For the soil within the root zone, the values of K_{sm} (0.018 m/day in D36, and 0.075 m/day in D320 soils) are in the same magnitude as those for the bare soil (0.075 m/day). The K_{sm} for the low planting density soil (0.018 m/day in D36) is lower than the K_s (0.075 m/day) of the bare soil, and this may be related to the occupations of the live roots (Ng et al. 2016a).

In the dual-permeability model, the hydraulic interaction between the matrix and preferential flow domains is governed by the water exchange term Γ_w in Eq. (7). The water exchange rate between these two domains depends on the parameterization of α_w. For a larger α_w, an equilibrium of pore water pressure between the matrix and preferential flow domains required would reach more quickly. In this study, moderate values of α_w of 25 and 15 m^{-2} are used for the low and high planting density soils, respectively. The use of a lower α_w for the high planting density soil may be related to the coating effects in biopores (Leue et al. 2010). The hydraulic interaction between root channel and soil matrix may be hampered by the non-wetting effects of soil organic matters (Jarvis 2007). Detailed calibration procedures of α_w for a given set of infiltration data through different parameterisation strategies are provided in Shao et al. (2015, 2016).

5 Results and Discussion

5.1 Infiltration rate and cumulative infiltration

The Infiltration rate and cumulative infiltration during the 2 h rainfall event are shown in Figure 4. The measurement shows that infiltration rate and amount in D320 are higher than those in D36. According to the study reported by Ng et al. (2016b), this is mainly attributed to two reasons. For the case of high planting density (D320), the intense competition between neighboring plants results in decayed roots (see Figure 2), hence creating preferential channels that facilitate infiltration. On the other hand, the live root biomass in the case of low planting density (D36) might have occupied the soil pore space, reducing the available pore size and infiltration capacity (Ng et al. 2016a).

Both the single- and dual- permeability models can simulate the same cumulative infiltration at the end of the rainfall event in both the cases (Figure 4), which is achieved by calibrating the saturated hydraulic conductivities. As expected, the infiltration rate decreases from a high value (close to the rainfall intensity) to a lower value (close to the saturated hydraulic conductivity) during the 2 h rainfall period, due to the decreased pressure gradient at the soil surface during the infiltration. Correspondingly, the cumulative infiltration is generally approaching to a nearly constant increasing rate.

The single- and dual- permeability models could simulate infiltration rate well for the case of low planting density (D36). On the contrary, much greater differences between two models can be found when simulating infiltration rate and cumulative infiltration for the case of high planting density (D320). Infiltration rate and cumulative infiltration in high planting density soil is much higher than that in low planting density soil, and this can be modelled using a high value of w_f to describe a higher soil moisture storage in preferential flow domain. At 50 min, for instance, the difference between the measured and simulated infiltration amount by the dual-permeability model is less than 15%, but such difference is more than 50% using the single-permeability model (Figure 4b). The dual-permeability model captures the infiltration behavior better for both low and high planting density soils, while the occurrence of preferential water flow may more significantly affect the infiltration rate and cumulative infiltration for the case of high planting density.

5.2 Pore water pressure profile after rainfall

Figure 5 compares the measured and simulated pore water pressure before and after 1 and 2 h of rainfall, respectively. Considering that the tensiometers used in the experiments were used to record matric suction in the soil matrix, the pore water pressure in the matrix domain p_m

($= \gamma_w h_m$) simulated by the dual-permeability model is used for comparison. The initial profile of pore water pressure before rainfall is the result of the 4-day drying (i.e., end of the first stage of the drum tests). Compared with the low planting density soil (D36), the pore water pressure in high planting density soil (D320) is significantly lower both within and below the root zone. This is attributed to the greater transpiration and plant root water uptake at high planting density, causing a significant reduction of soil moisture and pore water pressure.

After 1h or 2h rainfall, the increased pore water pressure in shallower depth is much more significantly than that in deeper depth, regardless of the planting density considered. After the rainfall, the maximum depth of pressure response in D320 can be up to the depth of 0.35 m, whereas that in D36 is shallower than 0.25 m depth. The observed pore water pressure responses are consistent with the responses of infiltration rates (Figure 4). Higher infiltration rate in D320 leads to a greater increase in pore water pressure, more cumulative infiltration, higher infiltration rate, and hence deeper infiltration depth.

Simulated results from the single-permeability model show that, after 1 or 2 h rainfall, there are clear wetting fronts within which the pore water pressure increases significantly. The pore water pressure below remains unchanged. However, the single-permeability model overestimates the pore water pressure within the wetting front, and underestimates the infiltration depth for both cases of D36 and D320. The considerable changes of pore water pressure in deeper depth during the rainfall tests cannot be simulated by the single-permeability model. On the contrary, the dual-permeability model appears to give a better match with the measurements of the pore water pressure profiles for the entire depth after 1 and 2 h of rainfall, despite of a slight overestimation of the pressure at 0.15 m in D320. The deeper pore water pressure response observed in the experiments can be captured by the dual-permeability model, especially for the high planting density soil where preferential flow may be more significant.

5.3 Hydrological processes simulated by single-permeability model

The simulated vertical profiles of soil water content and pore water pressure during the 2 h infiltration period by the single-permeability model is shown in Figure 6. The simulation results show that by using the single-permeability model, a clear piston-shape wetting front advancement can be identified from soil moisture and pore water pressure profiles in both the low and high-planting density soils.

In low planting density soil (D36), the wetting fronts advance progressively downwards with time. After 25 min of rainfall infiltration, the wetting front reaches the depth of 0.05 m, and soil at the top 0.02 m becomes fully saturated. When rainfall continues from 25 to 120 min, the wetting front advances nearly at a constant velocity. The maximum depth of water infiltration after the rainfall is 0.11 m, and only the soil of the top 0.08 m is fully saturated. There is no build-up of positive pore water pressure head, because the wetting front does not reach the second soil layer (below the root zone) where the hydraulic conductivity is lower.

For the high planting density soil (D320), even though the values of initial soil water content and pressure are lower than those in the low planting density soil, the variation of wetting front with time is similar. The only difference is the velocity of the wetting front advancement. In high planting density soil (D320), due to the higher infiltration rate (Figure 4), the rate of wetting front advancement is relatively faster, extending the saturated zone to a deeper depth of 0.14 m (compared to the depth of 0.09 m found in D36 soils). However, the pressure build-up is still insignificant.

5.4 Hydrological processes simulated by dual-permeability model

Figure 7 shows the simulated water content and pressure in the matrix and preferential flow domains, and the water exchanges between the two domains for the low planting density soil (D36). Before rainfall, there is no water exchange between domains (Figure 7f), because the initial pressure distributions in the matrix and preferential flow domains are the same. After 2 min rainfall, most of the rainwater infiltrates into the preferential flow domain, as the rainfall intensity surpasses the infiltration capacity of the matrix domain. Consequently, the wetting front in the preferential flow domain propagates with a relatively high velocity, as revealed by the rapid increase of water content and pore water pressure in the deep soil (Figures 7a, d). This implies that the preferential flow dominants the rainwater transport in soil. This phenomenon becomes more significant after 5-min rainfall, indicating by the highest water exchange at the depth of 0.05 m in Figure 7f.

Pressure build-up in the preferential flow domain starts when the wetting front propagates beyond the rooting depth (at 0.16 m depth in D36). Below the root zone, the soil is less permeable. After raining for 30 min, the advancement of the wetting front is relatively slower, and the simulated pore water pressure in the preferential flow domain p_f shows a steady

distribution (close to a hydrostatic distribution) within the root zone. At the end of the rainfall, the final infiltration depth of rainwater reaches 0.3 m.

Figure 8 shows the simulated distributions of soil water content and pore water pressure by using the dual-permeability model for the high planting density soil (D320). The initial soil water content and pore water pressure in this case are significantly lower than that in the case of low planting density (D36), because of higher transpiration rate. At the beginning of infiltration (t = 2 min), a significant fraction of rainwater infiltrates to the matrix domain (Figures 8 a, b), while the water exchange rates along the soil profile are nearly zero. After 2 min of rainfall when infiltration capacity of the matrix domain has reached, rainwater starts to infiltrate into the preferential flow domain. Afterwards, the preferential flow dominates the pressure propagation. The difference in pore water pressure between the two domains results in the water exchange from the preferential flow domain to the matrix domain.

The final infiltration depth after 2 h rainfall for the case of high planting density (D320) is 0.35 m, which is deeper than that in D36 (0.3 m). This is because the cumulative infiltration is higher in the high planting density soil (Figure 4). The infiltrated rainwater may transport through the preferential flow path and more predominantly affect the deeper soil pressure response than the case in low planting density.

Overall, the dual-permeability model can capture the pressure response not only within, but also below the root zone. Under the applied heavy rainfall (73 mm/h), the wetting front of the preferential flow is deeper than that of the matrix flow, causing a fast and significant pressure build-up for almost the entire soil profile that cannot be captured by the single-permeability model. Interestingly, the soil in the matrix domain between the depths of 0.1 to 0.3 m remains largely unsaturated – a hydrological process often called bypass flow. Although there are substantial increases of water content and pore water pressure in deeper soil depths, the non-equilibrium between the matrix and the preferential flow domains are revealed to be different in low and high planting density soils. The simulations using the dual-permeability model show that the preferential flow could lead to more significant responses of water content, and the increase of pore water pressure in the high planting density soil is larger than those in the low planting density soil.

5.5 Preferential flow effects on slope stability

The stability of infinite vegetated slopes with a gradient of 28° is analysed. The mechanical properties of the CDG soils used in the drum tests were reported by Liu et al. (2015). The effective cohesion of the CDG is 0 kPa, while the effective friction angle is 37.4°. The effective cohesion contributed by mechanical root reinforcement was set to a relatively low value of 2 kPa and is assumed to be constant and distributed uniformly within the root zone. The values of factor of safety (F_s) of the vegetated slopes with two planting densities (i.e., D36 and D320) were calculated by combining the infinite slope stability modelling approach (Eq. 14 – 16) with the single- or dual- permeability models.

The calculated profiles of F_s before and after 2h rainfall are shown in Figure 9. When using the single-permeability model, the simulated pore water pressure (Figures 6b, d) can be used as an input to Eq. 14 for calculating its corresponding F_s. For the calculation of F_s using the dual-permeability model (with $p_{eff} = p_f$), the simulated pore water pressure in the preferential flow domain (Figures 7d, 8d) was substituted into Eq. 14 – 16. The pressure build-up and the wetting front advancement by the preferential flow were much more significant than in the matrix flow domain. Therefore, using p_f to calculate F_s could provide a more conservative assessment of the slope stability.

Before rainfall, the F_s calculated by the two models are identical to each other. The F_s in the high planting density slope (D320) is much higher than that of the low planting density slope (D36) because of the reduction of pore water pressure by evapotranspiration. After 2 h of rainfall, the F_s calculated by the single-permeability model is larger than 1.0 along the entire soil profile, regardless of the planting density considered. This means that no slope failure exists in both cases. It can be seen that the decrease of F_s happened mainly within the wetting front, where the pore water pressure increases significantly (refer to Figure 6). The volume of soil being affected is found to be greater in the slope with high planting density because of the increased infiltration rate (refer to Figure 4). In contrast, F_s below the wetting front remains unchanged. As has been revealed from the comparison shown in Figure 5, the use of the single-permeability model may underestimate the pore water pressure in deep soil compared with the measurement, due to its inability to capture preferential flow that might have taken place in the vegetated soils. This highlights the importance of having the preferential flow to

be captured when assessing pore water pressure distributions in vegetated soil, in order to prevent overestimation, hence less conservative, on slope stability calculation.

With the assumption of $p_{eff} = p_f$, the calculated F_s by the dual-permeability model is lower than that calculated by the single-permeability model. The relatively high F_s in very shallow depth is contributed by the mechanical root reinforcement, despite of the low effective cohesion provided by roots of 2 kPa. Near and slightly below the interface between rooted and bare soil, the dual-permeability model predicts F_s to be lower than 1.0, indicating a potential slope failure. This is attributed to the relatively rapid pore water pressure build-up due to the presence of preferential flow. Such preferential flow appears to exist in both the low and high planting density soils, but it is comparatively more significant for the latter case due to the much higher cumulative infiltration and infiltration rate (Figure 2 and 4). The more decayed roots in the high planting density soil would result in more infiltration and larger value of pressure build-up, which adversely affects the slope stability. However, it should be noted that setting p_{eff} to be p_f represents a worst-case scenario that may lead to a rather conservative calculation of factor of safety.

5.6 Discussion about the choice of effective pressure for slope stability calculation

In a heterogeneous soil where preferential flow could happen, it remains unknown about the relative contribution of pore water pressure between the matrix domain and preferential flow domains to the soil shear strength. Most of the existing hydro-mechanical models use single-permeability model to calculate pore water pressure in soil matrix for slope stability analysis. When coupling a dual-permeability model (which adopts a dual-continuum approach) with a slope stability model, using the pore water pressure of p_f or p_m may lead to different results in slope stability calculations. Instead of using p_f as p_{eff} to calculate F_s (as have been shown in Figure 9), it may be necessary to investigate how different choices of p_{eff} would affect F_s.

Comparison of F_s calculated by using different p_{eff} (i.e., p_f, p_m, or their arithmetic mean ($0.5*(p_f + p_m)$) is given in Figure 10. As expected, regardless of the planting density, the calculated profile of F_s using p_m is much higher than that calculated one using p_f, because the pore water pressure in the matrix domain is significant higher than that in the preferential domain (see Figures 8d, e and 9d, e). This suggests that it is less conservation for the stability calculation of vegetated soil to use p_m to completely ignore the effects of preferential flow.

In an attempt to examine the combined effects of p_f and p_m on p_{eff} and slope stability, the calculated F_s using the arithmetic mean (i.e., $0.5*(p_f + p_m)$) is obtained for both the low and high planting density soils in Figure 10. As expected, the calculated F_s in both cases falls between the values obtained by either p_f or p_m, though the F_s tends to be closer to the latter case. Note that the above calculation has made an assumption on the equal weighting on the contribution of p_f and p_m to shear strength. As far as the authors are aware, the exact weighting is not known and it is believed to be dependent on the geometry, location, and distribution of the preferential flow channels and potential failure surface. More detailed investigation to correlate preferential flow with soil shear strength is needed in the future.

6. Summary and concluding remarks

Effects of plant-induced preferential flow on soil hydrology and slope stability were explored through experimental and numerical modelling approaches in this study. Rainfall infiltration tests were conducted in compacted silty sand vegetated plots with a selected tree species, *Schefflera heptaphylla*, with two different planting densities (i.e., high planting density 320 seedlings/m^2 and low planting density 36 seedlings/m^2). Post-test reconstruction of the plant root systems suggested that root decaying in the high planting density soils was much more evident than that in the low planting density soils. In order to capture the effects of root decaying on preferential flow, two numerical models were implemented to simulate the infiltration tests: one is the single-permeability model (which uses one Darcy-Richards equation to consider matrix flow-only), and another is the dual-permeability model (which couples two modified Darcy-Richards equations to simulate both matrix and preferential flow). The calibrated hydrological models were further used to evaluate the effects of plant-induced preferential flow on the stability of infinite vegetated slopes.

The test results show that the planting density has significant effects on the shape of soil water retention curve (SWRC). The presence of decayed roots caused a decrease in air-entry pressure, while desorption and adsorption rates remain almost unchanged. The root-induced changes in SWRC were able to be captured by both the single- and dual- permeability models. The experiment also showed that the infiltration rate in high planting density soils was significantly higher, and this may be caused by the preferential flow along macropores created by decayed roots. The dual-permeability model, in which preferential flow could be modelled by the dual-continuum approach, showed a closer match with the measurements than the

single-permeability model. The single-permeability model however significantly underestimated the infiltration rate at the beginning of rainfall (0-20min) and then overestimated during the last period (80-120 min).

Considering both preferential flow and matrix flow domains when using the dual-permeability model showed that preferential water flow was likely to take place in both low and high planting density. The preferential flow effects appeared to be more significant in the high planting density soil because of the greater increase in pore water pressure and deeper depth of infiltration. These hydrological processes were, however, not possible to be captured by the single-permeability model due to its inability to simulate the preferential flow effect using the matrix flow domain alone. Instead, the single-permeability model simulated the piston-shape of wetting front advancement during rainfall, which resulted in significant under-prediction of infiltration depth and overestimation of the pore water pressure within the root zone.

Because of the inability of the single-permeability model, a less conservative calculation of slope stability is resulted. Regardless of the planting density considered, the single-permeability model estimated significantly higher factor of safety than the dual-permeability model, especially on the deeper soil depths below the root zone. In contrast, when the dual-permeability model was used, a lower factor of safety is resulted. While the shallow stability of the vegetated slopes (up to 0.1 m depth within the root zone) is mainly provided by the mechanical root reinforcement, the factor of safety below the root zone is marginally closer to 1. Although the dual-permeability model is better captured the variations of pore water pressure in vegetated soils, caution should be taken on the choice of effective pressure for this model when assessing the factor of safety. Simulation using the pore water pressure in the preferential flow domain and the matrix domain in the model would result in over- and under-conservative assessment of the stability of vegetated slopes, respectively.

Acknowledgements

Research grants HKUST6/CRF/12R provided by the Research Grants Council of the Government of the Hong Kong SAR is acknowledged. The first author is financially supported by the scholarship (No. 2011671055) provided by the China Scholarship Council. The third author would also like to acknowledge the EU Marie Curie Career Integration Grant

under the project 'BioEPIC slope' and research travel support from the Northern Research Partnership (NRP).

References

Azam-Ali, S. N., Gregory, P. J., and Monteith, J. L. 1984. Effects of planting density on water use and productivity of pearl millet (Pennisetum typhoides) grown on stored water: growth of roots and shoots. Experimental Agricultural, **20**(3): 203–214.

Benomar, L., DesRochers, A., and Larocque, G. 2012. The effects of spacing on growth, morphology and biomass production and allocation in two hybrid poplar clones growing in the boreal region of Canada. Trees – Structure and Function, **26**(3): 939–949.

Beven, K., and Germann, P. 2013. Macropores and water flow in soils revisited. Water Resources Research, **49**(6): 3071–3092.

Bogaard, T. A., and Greco, R. 2016. Landslide hydrology: from hydrology to pore pressure. Wiley Interdisciplinary Reviews: Water **3**(3): 439-459.

Cohen, D., Lehmann, P., and Or, D. 2009. Fiber bundle model for multiscale modeling of hydromechanical triggering of shallow landslides. Water Resources Research, **45**(10): W10436.

Darawsheh, M. K., Khah, E. M., Aivalakis, G., Chachalis, D., and Sallaku, F. 2009. Cotton row spacing and plant density cropping systems I. Effects on accumulation and partitioning of dry mass and LAI. Journal of Food Agricultural and Environment, **7**(3–4): 258–261.

Durner, W. 1994. Hydraulic conductivity estimation for soils with heterogeneous pore structure. Water Resources Research, **30**(2): 211-223.

Dusek, J., Gerke, H. H., and Vogel, T. 2008. Surface Boundary Conditions in Two-Dimensional Dual-Permeability Modeling of Tile Drain Bromide Leaching. Vadose Zone Journal, **7**(4): 1287–1301.

Feddes, R. A., Kowalik, P., Kolinska-Malinka, K., and Zaradny, H. 1976. Simulation of field water uptake by plants using a soil water dependent root extraction function. Journal of Hydrology, **31**(1): 13 – 26.

649 Gerke, H. H., and Köhne, J. M. 2004. Dual-permeability modeling of preferential bromide
650 leaching from a tile-drained glacial till agricultural field. Journal of Hydrology, **289**(1): 239–
651 257.

652 Gerke, H. H., and van Genuchten, M. 1993. Evaluation of a first-order water transfer term for
653 variably saturated dual-porosity flow models. Water Resources Research, **29**(4): 1225–1238.

654 Ghestem, M., Sidle, R. C., and Stokes, A. 2011. The influence of plant root systems on
655 subsurface flow: implications for slope stability. Bioscience, **61**(11): 869–879.

656 Hencher, S. R. 2010. Preferential flow paths through soil and rock and their association with
657 landslides. Hydrological Processes, **24**(12): 1610–1630.

658 Iverson, R. M. 2000. Landslide triggering by rain infiltration. Water Resources Research,
659 **36**(7): 1897–1910.

660 Jarvis, N. J. 2007. A review of non-equilibrium water flow and solute transport in soil
661 macropores: principles, controlling factors and consequences for water quality. European
662 Journal of Soil Science, **58**(3): 523–546.

663 Köhne, J. M., Köhne, S., and Gerke, H. H. 2002. Estimating the hydraulic functions of dual-
664 permeability models from bulk soil data, Water Resources Research, **38**(7): doi:10.1029/
665 2001WR000492, 2002.

666 Köhne, J. M., Köhne, S., and Šimůnek, J. 2009. A review of model applications for structured
667 soils: a) Water flow and tracer transport. Journal of Contaminant Hydrology, **104**(1–4): 4–35.

668 Krzeminska, D. 2012. The influence of fissures on landslide hydrology, TU Delft, Delft
669 University of Technology.

670 Leue, M., Ellerbrock, R. H., and Gerke, H. H. 2010. DRIFT Mapping of Organic Matter
671 Composition at Intact Soil Aggregate Surfaces. Vadose Zone Journal, **9**(2): 317–324.

672 Lehmann, P., and Or, D. 2012. Hydromechanical triggering of landslides: From progressive
673 local failures to mass release. Water Resources Research, **48**(3): W03535

674 Leung, A. K., Coo, J. L., Ng, C. W. W., and Chen, R. 2016. New transient method for
675 determining soil hydraulic conductivity function. Canadian Geotechnical Journal, **53**(8): 1332
676 – 1345

677 Leung, A. K., Garg, A., and Ng, C. W. W. 2015a. Effects of plant roots on soil-water
678 retention and induced suction in vegetated soil. Engineering Geology, **193**: 183–197.

679 Leung, A. K., Garg, A., Coo, J. L., Ng, C. W. W., and Hau, B. C. H. 2015b. Effects of the
680 roots of *Cynodon dactylon* and *Schefflera heptaphylla* on water infiltration rate and soil
681 hydraulic conductivity. Hydrological Processes, **29**(15): 3342 – 3354.

682 Li, Y., and Ghodrati, M. 1994. Preferential transport of nitrate through soil columns
683 containing root channels. Soil Science Society of American Journal, **58**: 653–659.

684 Liu, H. W., Feng, S., and Ng, C. W. W. 2016. Analytical analysis of hydraulic effect of
685 vegetation on shallow slope stability with different root architectures. Computers and
686 Geotechnics, **80**: 115–120.

687 Lu, N., and Godt, J. 2008. Infinite slope stability under steady unsaturated seepage conditions.
688 Water Resources Research, **44**(11): W11404.

689 Lu, N., Godt, J. W., and Wu, D. T. 2010. A closed-form equation for effective stress in
690 unsaturated soil. Water Resources Research, **46**(5): W05515.

691 Lu, N., Şener-Kaya, B., Wayllace, A., and Godt, J. W. 2012. Analysis of rainfall-induced
692 slope instability using a field of local factor of safety. Water Resources Research, **48**(9):
693 W09524.

694 Ng, C. W. W., and Menzies, B. 2007. Advanced unsaturated soil mechanics and engineering.
695 London, UK: Taylor & Francis.

696 Ng C. W. W., and Leung A. K. 2012. Measurements of drying and wetting permeability
697 functions using a new stress-controllable soil column. Journal of Geotechnical and
698 Geoenvironmental Engineering, **138**(1): 58–68.

699 Ng, C. W. W., Leung, A. K., and Woon, K. X. 2014. Effects of soil density on grass-induced
700 suction distributions in compacted soil subjected to rainfall. Canadian Geotechnical Journal,
701 **51**(3): 311–321.

702 Ng, C. W. W., Ni, J. J., Leung, A. K., and Wang, Z. J. 2016a. A new and simple water
703 retention model for root-permeated soils. Géotechnique letters, **6**(1) : 106 – 111.

Ng, C. W. W., Ni, J. J., Leung, A. K., Zhou, C., and Wang, Z. J. 2016b. Effects of planting density on tree growth and induced soil suction. Géotechnique, **66**(9): 711–724.

Nieber, J. L., and Sidle, R.C. 2010. How do disconnected macropores in sloping soils facilitate preferential flow? Hydrological Processes, **24**(12):1582–1594.

Nimmo, J. R. 2007. Simple predictions of maximum transport rate in unsaturated soil and rock. Water Resources Research, **43**(5): W05426.

Nimmo, J. R. 2012. Preferential flow occurs in unsaturated conditions. Hydrological Processes, **26**(5): 786-789.

Scanlan, C. A., and Hinz, C. 2010. Insight into the processes and effects of root induced changes to soil hydraulic properties. Proceedings of the 19th world congress of soil science, soil solutions for a changing world, Brisbane, Australia, vol. 2, pp. 41–44.

Scholl, P., Leitner, D., Kammerer, G., Lioskandl, W., Kaul, H. P., and Bodner, G. 2014. Root induced changes of effective 1D hydraulic properties in a soil column. Plant and Soil, **381**(1–2), 193–213.

Shao, W., Bogaard, T., and Bakker, M. 2014. How to Use COMSOL Multiphysics for Coupled Dual-permeability Hydrological and Slope Stability Modeling. Procedia Earth and Planetary Science **9**: 83-90.

Shao, W., Bogaard, T., Bakker, M., and Berti, M. 2016. The influence of preferential flow on pressure propagation and landslide triggering of the Rocca Pitigliana landslide. Journal of Hydrology, online.

Shao, W., Bogaard, T. A., Bakker, M., and Greco, R. 2015. Quantification of the influence of preferential flow on slope stability using a numerical modelling approach. Hydrology and earth system Sciences, **19**(5): 2197– 2212.

Sidle, R. C., and Bogaard, T. A. 2016. Dynamic earth system and ecological controls of rainfall-initiated landslides. Earth-Science Reviews, **159**, 275– 291.

Sidle, R. C., Noguchi, S., Tsuboyama, Y., and Laursen, K. 2001. A conceptual model of preferential flow systems in forested hillslopes: evidence of self-organization. Hydrological Processes, **15**(10): 1675– 1692.

732 Sidle, R. C., Ochiai, H., Sidle, R.C., and Ochiai, H. 2013. Landslides: Processes, Prediction,
733 and Land Use, pp. 41-119, American Geophysical Union.

734 Simunek, J., Van Genuchten, M. T., and Sejna, M. 2005.The HYDRUS-1D software package
735 for simulating the one-dimensional movement of water, heat, and multiple solutes in
736 variably– saturated media, pp. 1– 240.

737 Snyder, K. A., Richards, J. H., and Donovan, L. A. 2003. Night-time conductance in C_3 and
738 C_4 specises: do plants lose water at night? Journal of Experimental Botany, **54**(383): 861 –
739 865.

740 Talebi, A., Uijlenhoet, R., and Troch, P. A. 2008. A low-dimensional physically based model
741 of hydrologic control of shallow landsliding on complex hillslopes. Earth Surface Processes
742 and Landforms, **33**(13): 1964 – 1976.

743 Uchida, T. 2004. Clarifying the role of pipe flow on shallow landslide initiation. Hydrological
744 Processes,**18**(2): 375– 378.

745 Van Asch, T. W. J., Buma, J., and Van Beek, L. P. H. 1999. A view on some hydrological
746 triggering systems in landslides. Geomorphology, **30**(1–2), 25– 32.

747 van Dam, J. C., and Feddes, R. A. 2000. Numerical simulation of infiltration, evaporation and
748 shallow groundwater levels with the Richards equation. Journal of Hydrology, **233**(1–4): 72–
749 85.

750 Van Genuchten, M. T. 1980. A closed-form equation for predicting the hydraulic conductivity
751 of unsaturated soils. Soil science society of America journal, **44**(5): 892– 898.

752 Vergani, C., and Graf, F. 2015. Soil permeability, aggregate stability and root growth : a pot
753 experiment from a soil bioengineering perspective. Ecohydrology, doi: 10.1002/eco.1686.

754 Wang, D., Kang, Y., and Wan, S. 2007. Effect of soil matric potential on tomato yield and
755 water use under drip irrigation condition. Agricaltural Water Management, **87**(2): 180–186.

756

Table 1. Soil hydraulic parameters for the single-permeability model (Single), and the dual-permeability model (Dual) for the matrix and preferential flow (PF) domains

Model	Soil	Depth (m)	Domain	w (-)	θ_r (-)	θ_s (-)	K_s (m/day)	a (m^{-1})	n (-)	l (-)	a_w (m^{-2})
Single	Bare	0-0.45	Total domain	-	0.1	0.3	0.075	5	1.25	0.5	-
	D36	0-0.16	Total domain	-	0.1	0.3	0.060	4	1.26	0.5	-
	D320	0-0.13	Total domain	-	0.1	0.3	0.175	6	1.37	0.5	-
Dual	D36	0-0.16	Matrix domain	0.9	0.1	0.29	0.018	5	1.25	0.5	25
			PF domain	0.1	0.1	0.39	4.5	6	1.50	0.5	
		0.16-0.45	Matrix domain	0.9	0.1	0.29	0.018	5	1.25	0.5	25
			PF domain	0.1	0.1	0.39	0.018	5	1.25	0.5	
	D320	0-0.13	Matrix domain	0.8	0.1	0.27	0.075	5	1.30	0.5	15
			PF domain	0.2	0.1	0.39	4.5	10	1.50	0.5	
		0.13-0.45	Matrix domain	0.8	0.1	0.27	0.075	5	1.25	0.5	15
			PF domain	0.2	0.1	0.39	0.115	5	1.25	0.5	

Note: for the single-permeability model, the hydraulic parameters for the soil below the root zone are specified to be the same as those for the bare soil.

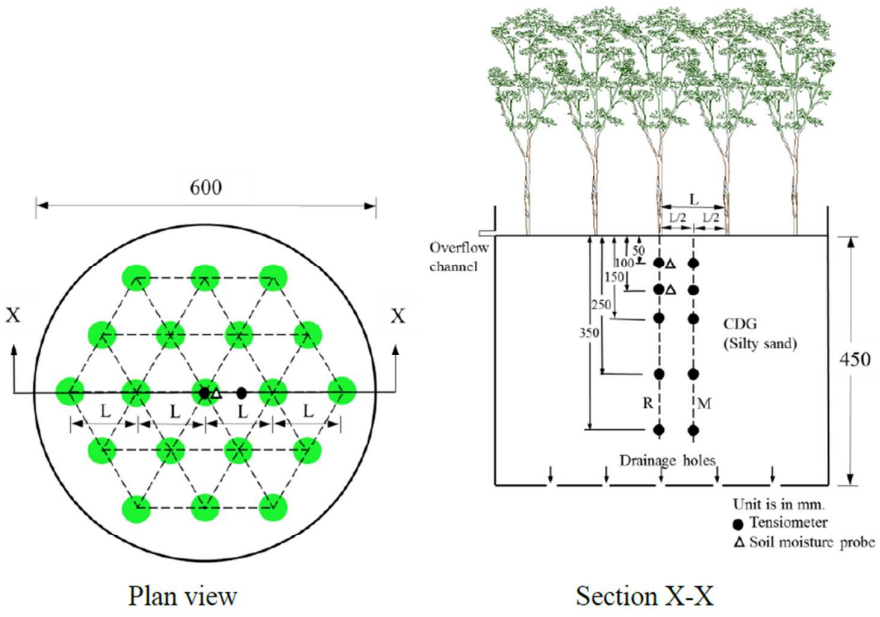

Figure 1. Schematic diagrams of a test drum and instrumentation (Ng et al., 2016b)

a. Low planting density D36

b. High planting density D320

c. Measured RAI

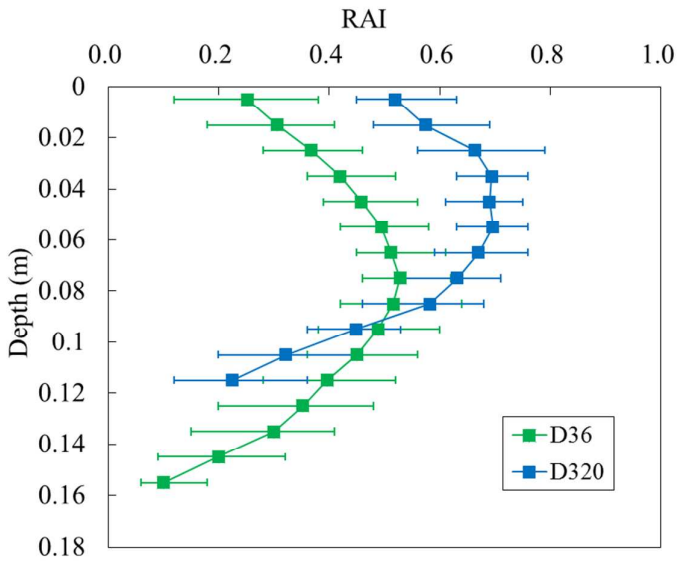

Figure 2. (a) Images of the root system for D36, (b) images of the root system for D320, (c) the measured RAI after a 4-month growing period (Ng et al., 2016b)

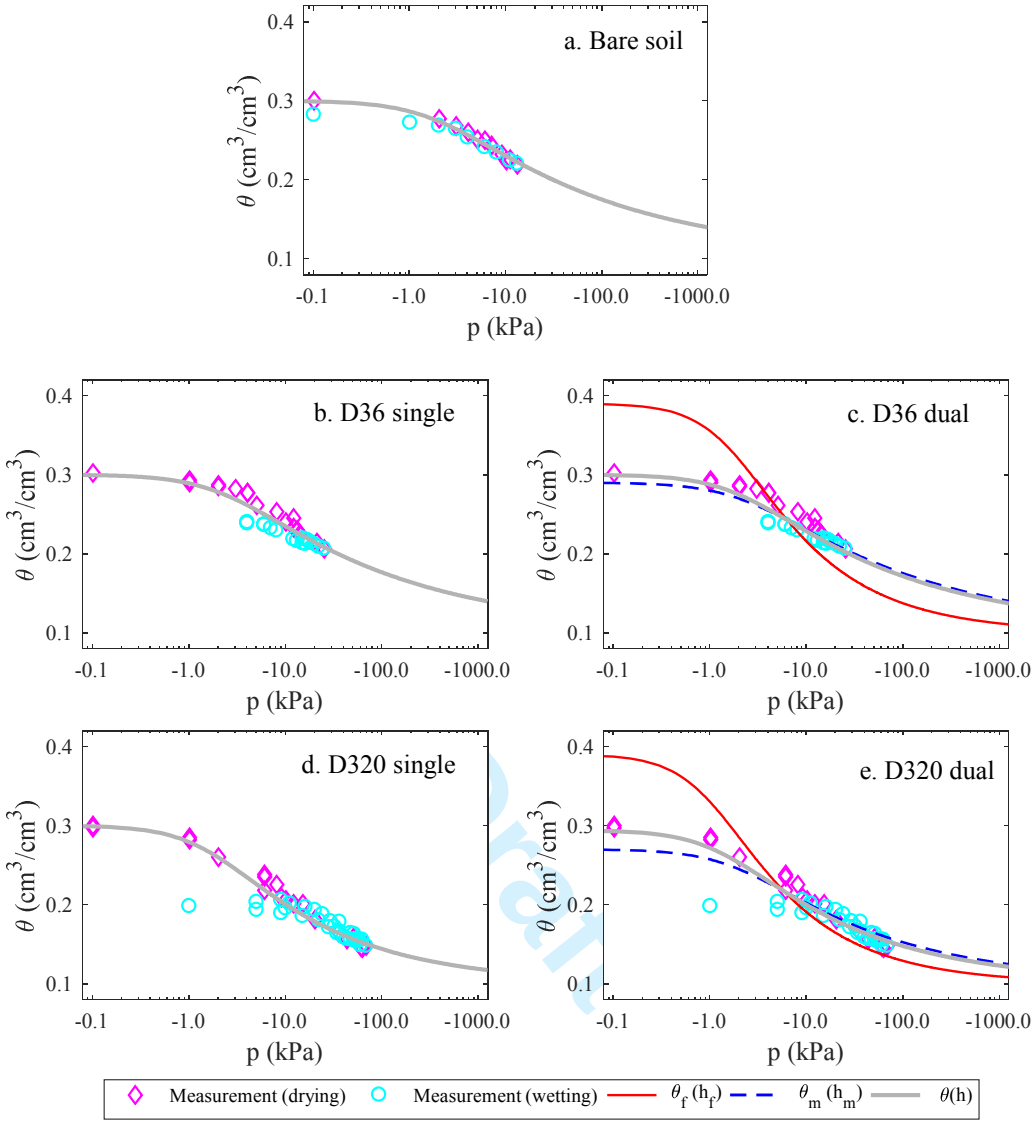

Figure 3. Soil water retention curve of (a) bare soil, (b) single- and (d) dual-permeability model in low planting density soil (D36), and (d) single- and (e) dual-permeability model in high planting density soil (D320)

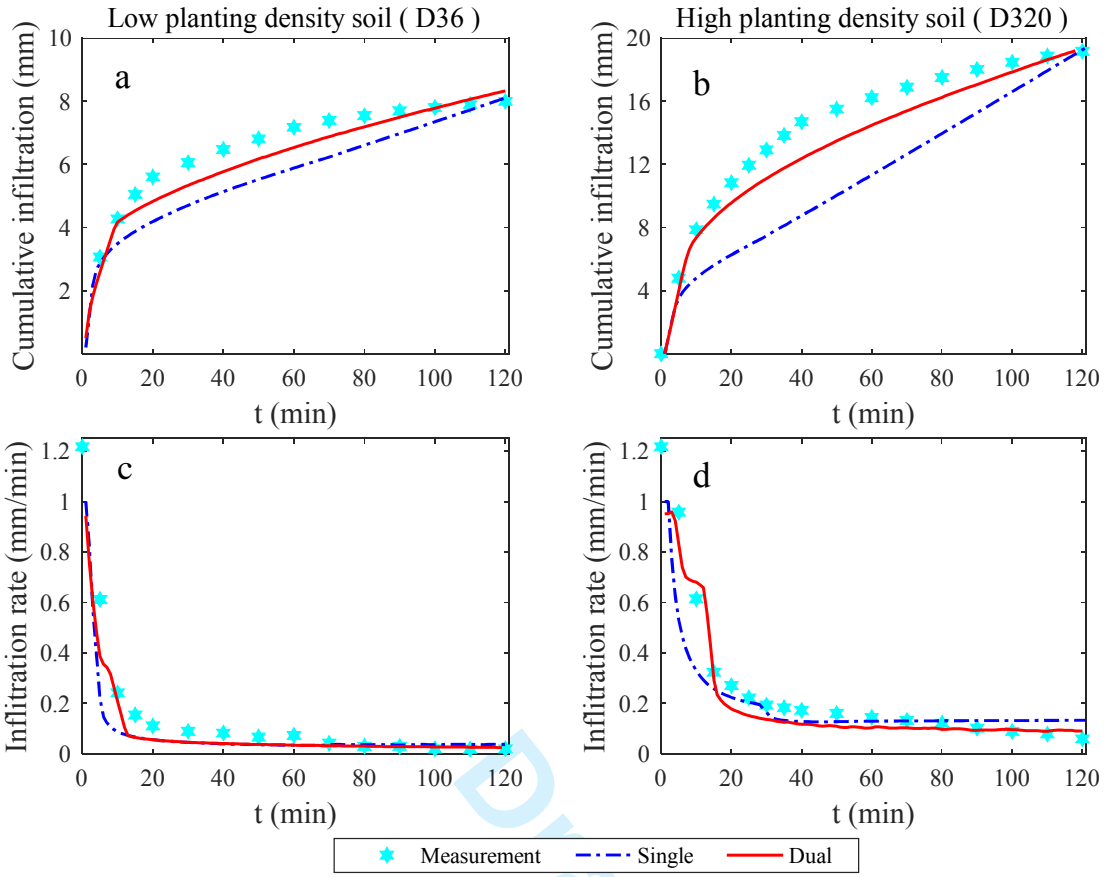

Figure 4. Comparison of the measurements (hexagram dots) and the simulations of cumulative infiltration and infiltration rate by the single- and dual- permeability models (lines) in low planting density soil D36 (left column) and high planting density soil D320 (right column)

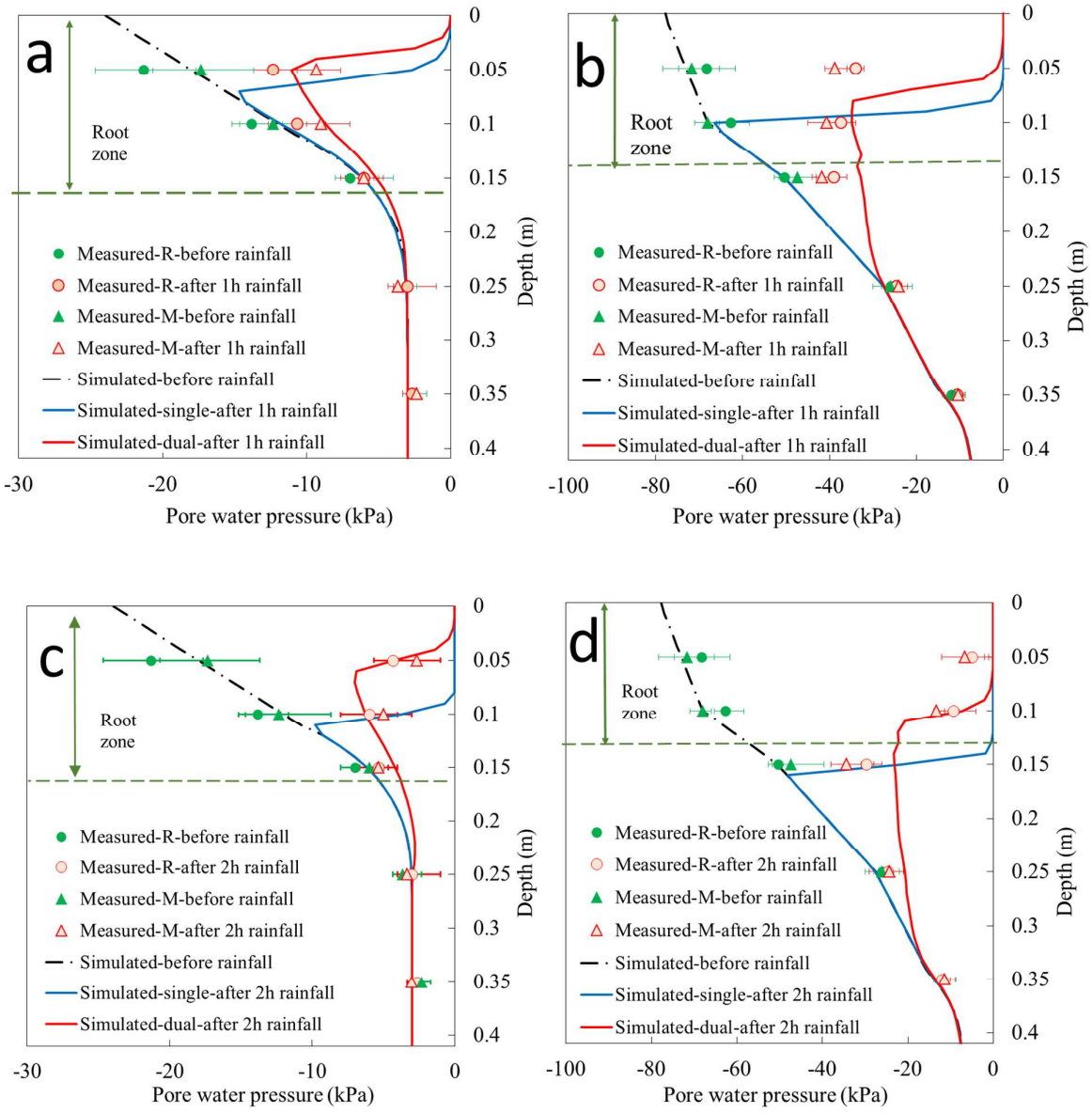

Figure 5. Comparison of the measured and simulated pore water pressure profiles by using the single- and dual- permeability models: (a) D36 and (b) D320 after1 h rainfall, and (c) D36 and (d) D320 at 2 h rainfall

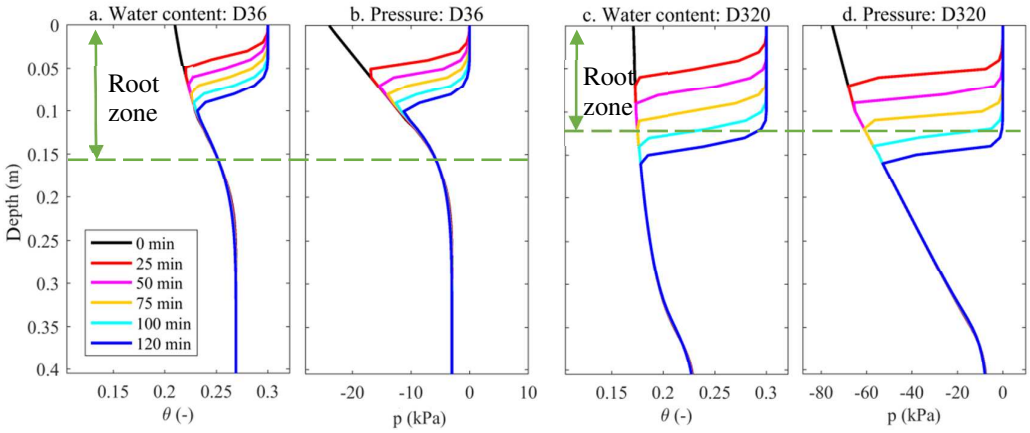

Figure 6. Simulated vertical profiles of soil water content (θ) and pore water pressure (p) in D36 and D320 soils by using the single-permeability model during the 2 hours of rainfall

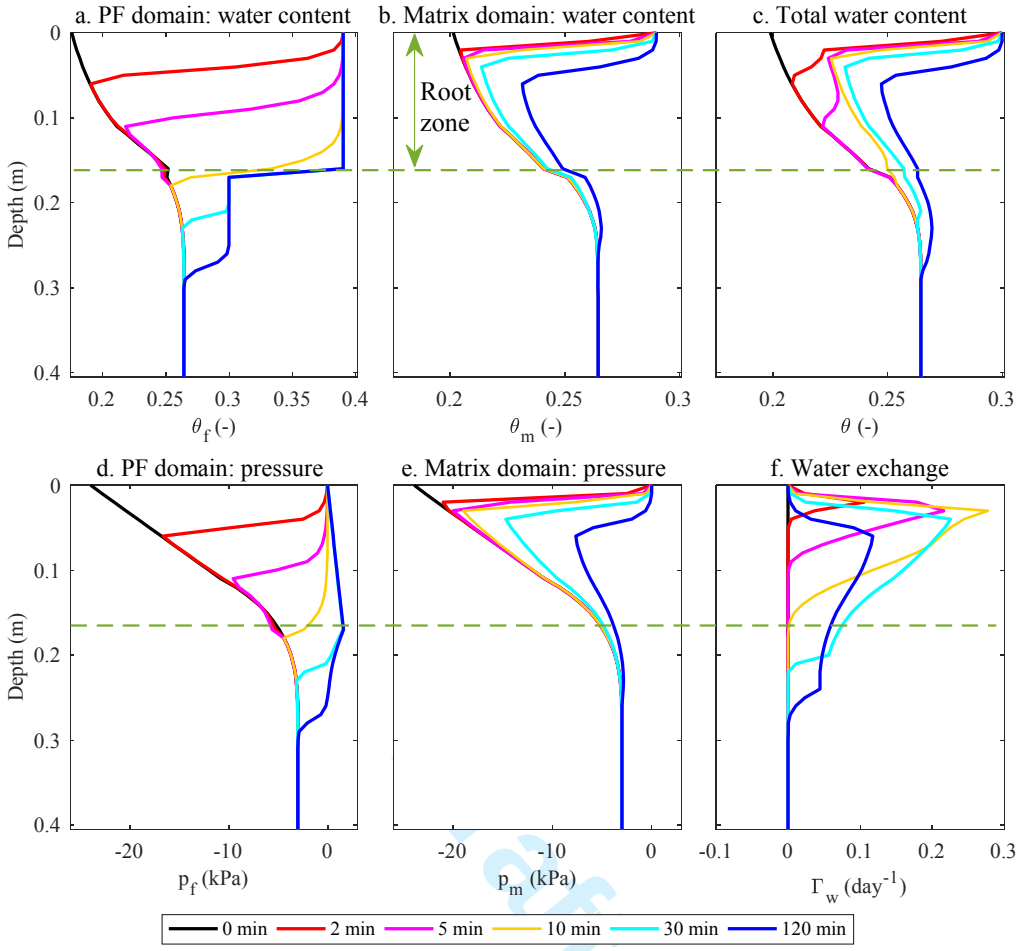

Figure 7. Simulated vertical profiles in D36 soil by the dual-permeability model during the 2 hours of rainfall: soil water content in (a) the matrix domain, (b) the preferential flow domain, and (c) the total domain; pore water pressure in (d) the matrix domain and (e) the preferential domain; and (f) the water exchange rate (positive denotes water exchange from the preferential flow domain to the matrix domain)

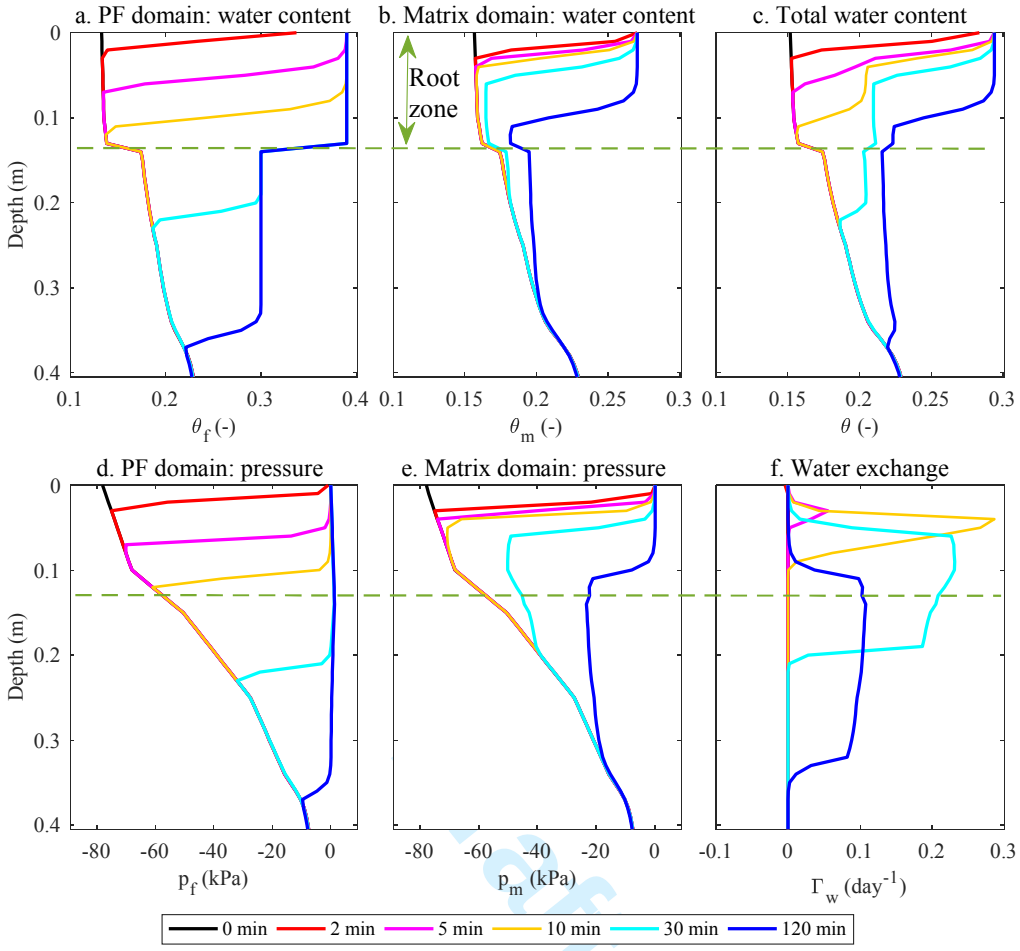

Figure 8. Simulated vertical profiles in D320 soil by the dual-permeability model during the 2 hours of rainfall: soil water content in (a) the matrix domain, (b) the preferential flow domain, and (c) the total domain; pore water pressure in (d) the matrix domain and (e) the preferential domain; and (f) the water exchange rate (positive denotes the water exchange from the preferential flow domain to the matrix domain)

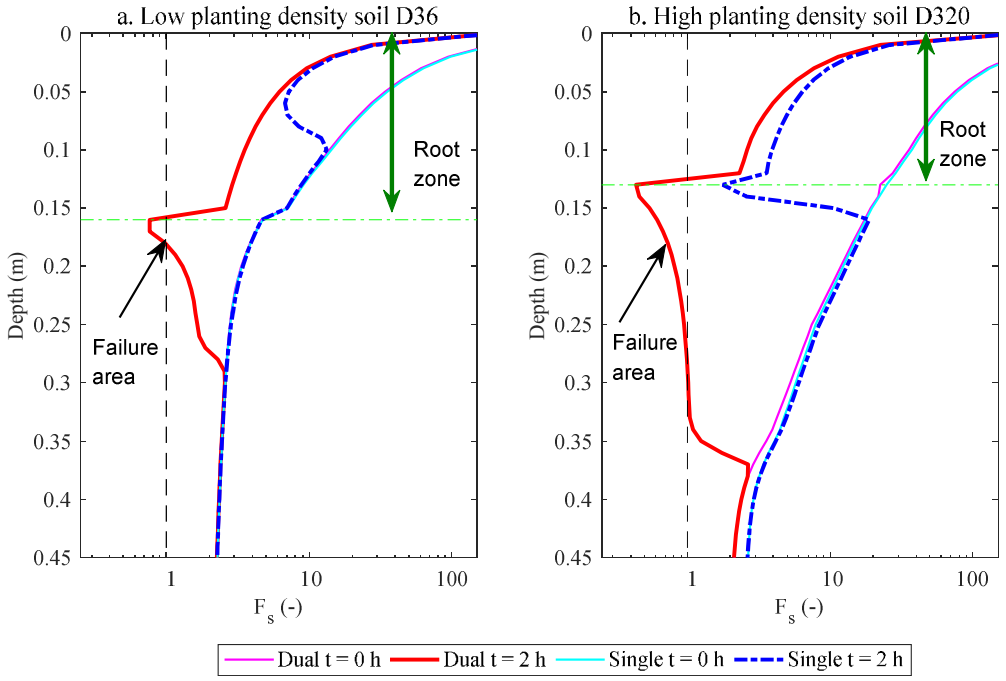

Figure 9. Effects of planting density on factor of safety (F_s) before and after the 2 h rainfall predicted by the single- and dual-permeability models (for $p_{eff} = p_f$)

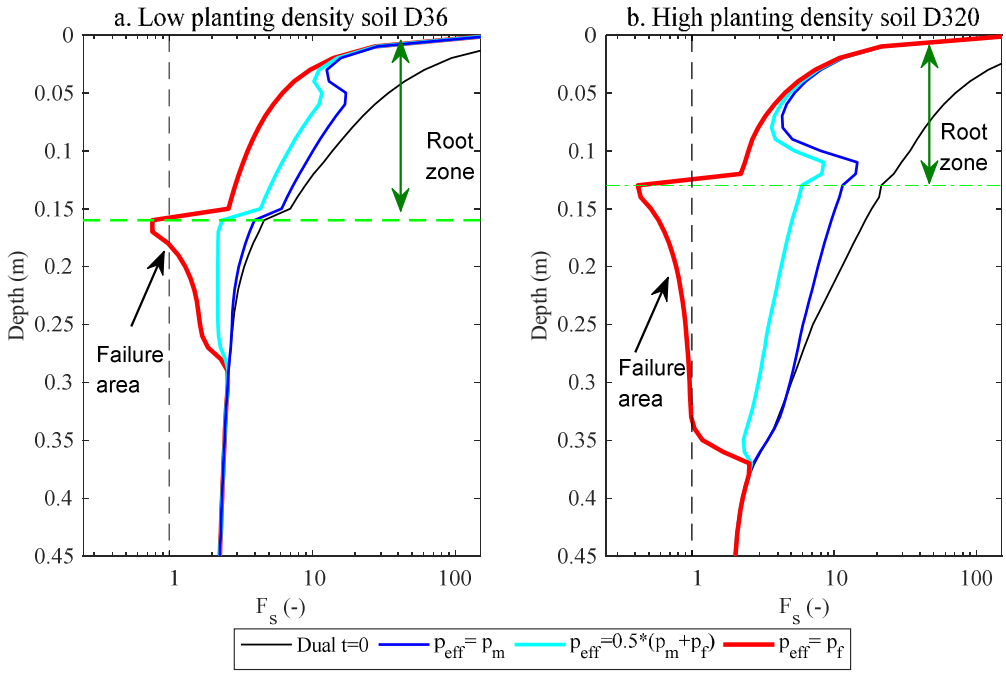

Figure 10. Effects of the choice of flow domain in the dual-permeability model on the slope stability